Roles of sterol glucosyltransferase and actin cytoskeleton in pexophagy of the methylotrophic yeast

Masahide OKU

2003

Roles of sterol glucosyltransferase and actin cytoskeleton in pexophagy of the methylotrophic yeast

Masahide OKU

2003

Contents

INTRODUCTION

Cytoplasmic constituents in any organism have to be properly degraded to maintain cellular homeostasis. Recently, extensive studies were made to elucidate the mechanism how the ubiquitin conjugation system recognizes a certain protein and transport it to proteasome, a cytosolic multifunctional protease complex (40). This system was found to ensure the normal progression of cell cycle, and regarded as an important factor of metastasis (cancer formation) (31).

Eukaryote cells are endowed with organelle degradation system termed autophagy whose central part (i.e. actual degradation process) is done in lysosome/vacuole compartment (10, 13, 17, 24, 25). In mammalian hepatocyte, autophagy comprises two types of membrane flux as to the transport of the target to lysosomes. One type undergoes the direct lysosomal engulfment of the cytoplasmic components (organelle or cytosol), which was named microautophagy. And the other type, termed macroautophagy, utilizes a-newly formed double-membrane structure to sequester the cytoplasmic compartments that subsequently fuses to lysosomal membrane. Either or both mechanisms occur depending on the cellular nutrient conditions. For instance, in hepatocytes, microautophagy is observed dominantly in basal (supplemented with rich nutrients) states, whereas macroautophagy is induced by nutrient deprivation. However, the molecular mechanisms of these degradation systems have been poorly elucidated.

A methylotrophic yeast *Pichia pastoris* has two

peroxisome-degradation systems (pexophagy), which belong to the two types of autophagy (34, 43, 44). After grown on methanol, this fungus can eliminate peroxisomes when the medium is shifted to either glucose or ethanol medium. Glucose adaptation leads to the induction of micropexophagy where vacuolar membrane changes its morphology to enwrap peroxisome cluster followed by the sequestration and degradation of the target organelle. And ethanol adaptation brings about macropexophagy, during which the formation of "macropexophagosome" in cytoplasm occurs to enwrap a peroxisome among the cluster and then the closed membrane structure fuses with vacuolar membrane to release the content into the lytic organelle.

The existence of micropexophagy is a unique feature of *P .pastoris* in that it is not observed in other methylotrophic yeasts (16, 41) or baker's yeast *Saccharomyces cerevisiae* (16). Therefore the study of this phenomenon in *P. pastoris* will give us important insights to understand the molecular mechanism of microautophagy that cannot be obtained by other yeasts.

In order to promote the morphological understanding of micropexophagy in *P. pastoris*, the author started this study with the overall depiction of organelle dynamics in micropexophagy shown in chapter I. Then the author focused on the two elements important for pexophagy in general, sterol glucosyltransferase and actin cytoskeleton. The studies on each element is reported and discussed in chapter II (sterol glucosyltransferase) and in chapter III (actin cytoskeleton).

CHAPTER I

Visualization and dissection of micropexophagic processes in a single cell

Introduction

In an earlier study (33), electron and fluorescent microscopy had shown that vacuolar membrane engulfment of peroxisome cluster occurred in a stepwise manner followed by the collapse of peroxisomes inside the vacuole. A model for micropexophagy progression was established from the observations. The overall processes were dissected into four stages (Stage 0 to 3) and the engulfment stage (Stage 1) was further divided to early and late sub-stages according to the extent to which vacuole enwrapped peroxisomes.

In order to confirm the validity of the working model and to understand the vacuolar membrane movements in more detail, it is necessary to chase the dynamics of the two organelles, vacuole and peroxisomes, in individual cells. Therefore the author devised a method to record the time-lapse images of the organelle morphology within an immobilized cell. Through this "single-cell" observation of micropexophagy, a new mode of vacuolar engulfment was discovered. Based on this, the author made a modification of original model for micropexophagy. The revised model fits better the actual images obtained with fluorescent microscopy of wild type and many micropexophagy-deficient (*paz* mutant) cells (26). The classification of

the *paz* mutants was done based on each of their morphological phenotypes, which will be discussed in relevance to the genetical features the mutants.

Materials and methods

Strains and media

A *P. pastoris* wild-type strain STW1 (PPY12 *his4*:: P_{AOX1}*GFP*-PTS1-*HIS4*) was used for time-lapse observation of vacuole and peroxisome during micropexophagy. The *paz* mutants were obtained through restriction enzyme-mediated integration of pREMI-Z vector. The integrated vectors with the flanking regions in *Pichia* genome were retrieved and re-introduced into STW1. The resultant strains were designated PZR1 to PZR13 according to the assigned *PAZ* numbers, which were subjected to morphological analyses. YPD (2% $_D$-glucose, 2% bacto-peptone and 1% yeast extract) and YNM medium (0.5% methanol, 0.05% yeast extract, 0.67% Yeast Nitrogen without amino acids and 0.2mg/L $_L$-arginine) were prepared with all the composites purchased from Difco.

Time-lapse observation of vacuole and peroxisome (Fig.1)

The cells that were grown on YNM medium for 12 h and labelled with FM4-64 (N-(3-triethylammmoniumpropyl)-4-(p-diethylamino-phenyl-hexatrienyl) pyridinium dibromide) were collected into 20μL of YPD medium and put on a coverslip which had been coated with 0.1% Concanavalin A (Wako chemical). After non-attached cells

were removed, the slip was layered and fixed with paper tape on a glassslide with YPD medium. This sample was continually (with 10 to 20 minute interval) subjected to observation by Zeiss Axioplan 2 fluorescence microscope. The images were captured with a Zeiss ZVS-47DE charged-coupled-device (CCD) camera using CG7 frame-grabber (Scioncorp).

Microscopy of *paz* mutants

The strains designated PZR1 (*paz1*) to PZR13 (*paz13*) were grown on YPD and transferred to YNM medium for 12 h. The cells were then transferred to YPD medium and subjected to observation at 0, 3, and 6 h after the YPD shift. The images were acquired as described above.

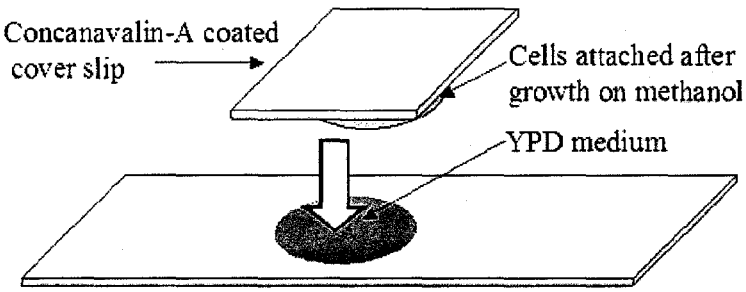

Fig.1 Outline of sample preparation for time-lapse observation of cells in micropexophagy.

Results

Two modes of vacuolar morphological dynamics during micropexophagy.

The author observed the continuous changes of vacuole and

peroxisome in each immobilized cell. Most of the observed cells showed morphological changes of vacuoles, and as shown in Fig.2, some of the cells accomplished the micropexophagic processes until the peroxisomal matrix-resident signal (GFP) diffused in the vacuole. This indicates that this observation experiment was able to trace the actual morphological changes of the organelles during micropexophagy.

The vacuolar engulfment of peroxisome cluster that had been presented in the statistical study (33) was successfully traced in this experiment (Fig.3A). In addition, another type of the vacuolar engulfment pattern was observed (Fig.3B). In this mode, a part of vacuolar membrane adjacent to the contact site with peroxisomes budded into a lobe that was still connected to the "mother" vacuolar membrane. After the lobe was formed, it eventually elongated along with the surface of the peroxisome cluster. It often gave birth to another lobe structure that also took part in the enwrapping of the peroxisomes. The elongation of the vacuolar lobes was terminated when the vacuolar membrane completely engulfed the whole part of peroxisome cluster.

Under our experimental conditions, approximately 70 % of the cells showed the engulfment pattern with the lobe formation (data not shown). As shown in Fig.2, the lobe-mediated vacuolar engulfment led to the GFP signal diffusion, confirming that this type of vacuolar movement is also a part of micropexophagic processes. Thus the author re-constructed the schematic model of micropexophagy as shown in Fig.4. In this model the vacuolar engulfment (Stage 1 to 2) was classified into two modes, one with the budding (lobe formation) step, designated as Stage 1b, and the other

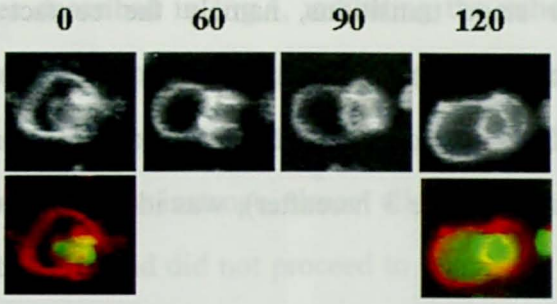

Fig.2 Micropexophagy completion observed in the mobilized cells.

The methanol-grown cells were immobilized and observed as described in Materials and Methods. The numbers indicate the time after the cells were transferred to the glucose medium (min).

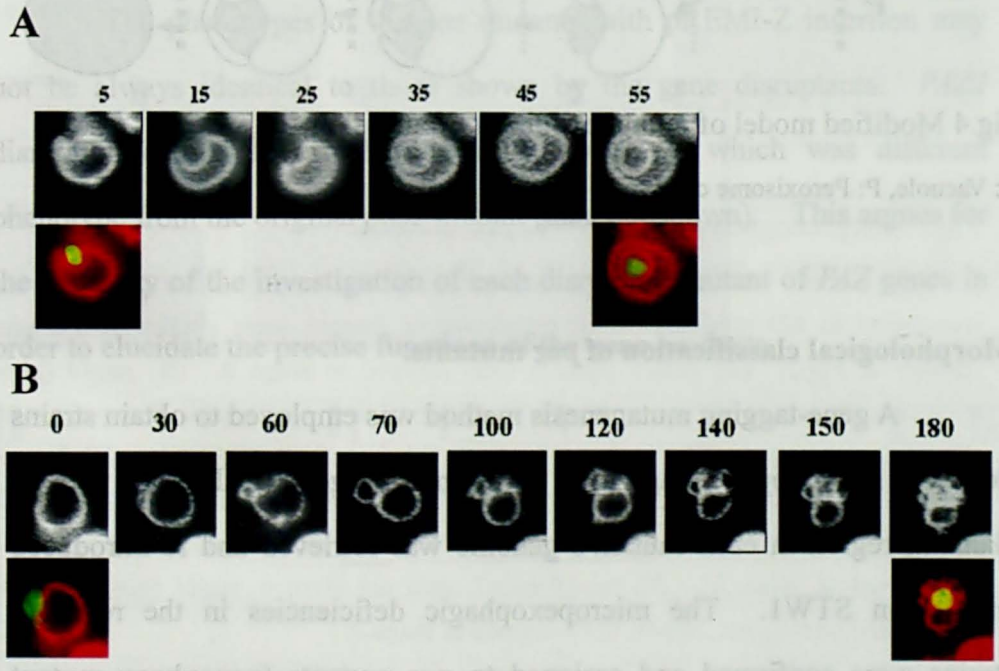

Fig.3 Two modes in vacuolar engulfment along with peroxisome cluster.

The vacuole and peroxisome morphology was observed as described in Fig.2. (A) The vacuole enwrapped the peroxisomes simply by invaginating its limiting membrane. (B) The vacuole engulfed the peroxisomes by continuous formation of lobe structure on the surface of the peroxisome cluster.

without the step. The other stage transitions, namely the contact of peroxisomes with spherical vacuolar membrane (Stage 0 to 1), the complete sequestration of peroxisomes from cytosol (Stage 2 to 3), and peroxisome collapse inside the vacuolar lumen (Stage 3 hereafter), was identical to the previous model.

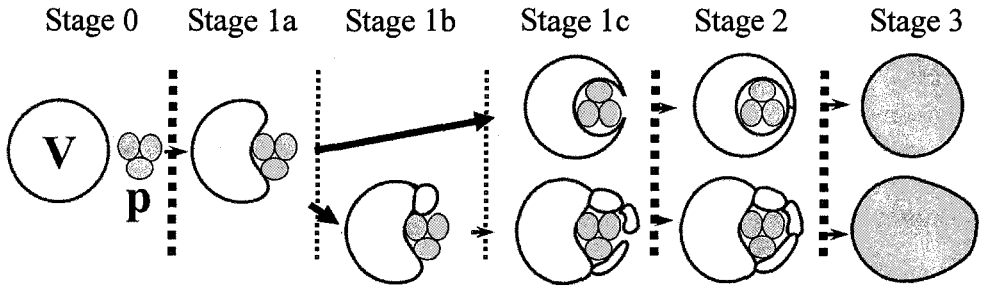

Fig.4 Modified model of micropexophagy progression.

V: Vacuole, P: Peroxisome cluster.

Morphological classification of *paz* mutants.

A gene-tagging mutagenesis method was employed to obtain strains defective in micropexophagy (26). The inserted gene (pREMI-Z) with its flanking region in each mutant's genome was retrieved and re-introduced into strain STW1. The micropexophagic deficiencies in the resultant strains were confirmed and assigned to *paz* mutants (pexophagy mutant among Zeocin resistant colonies).

In order to verify the schematic model constructed as shown in Fig.4, the morphology of the vacuole and peroxisomes was investigated in each *paz* mutant. Fig.5 shows the representative morphologies of the *paz* mutants 3h after the glucose shift. All the phenotypes fell into either of the

stages described in Fig.4, indicating the validity of the schematic model. Notably, the mutants of the same genetical group (such as *APG* or *GCN* homologues) showed the halt in micropexophagy at a similar stage transition. For instance, almost all the mutants of *APG* homologues ceased at Stage 1c, and did not proceed to Stage 2. And for the mutants of *GCN* family, the pathway seemed to be halted at Stage 2. These results suggest that the genes of the same family may act in accordance with each other to accomplish micropexophagy as well as other physiological functions (i.e., starvation-induced macroautophagy or general amino acid transcription).

The phenotypes of the *paz* mutants with pREMI-Z insertion may not be always identical to those shown by the gene disruptants. *PAZ2* disruption causes abnormal vacuolar morphology, which was different phenotype from the original *paz2* mutant (data not shown). This argues for the necessity of the investigation of each disruption mutant of *PAZ* genes in order to elucidate the precise functions of the gene products.

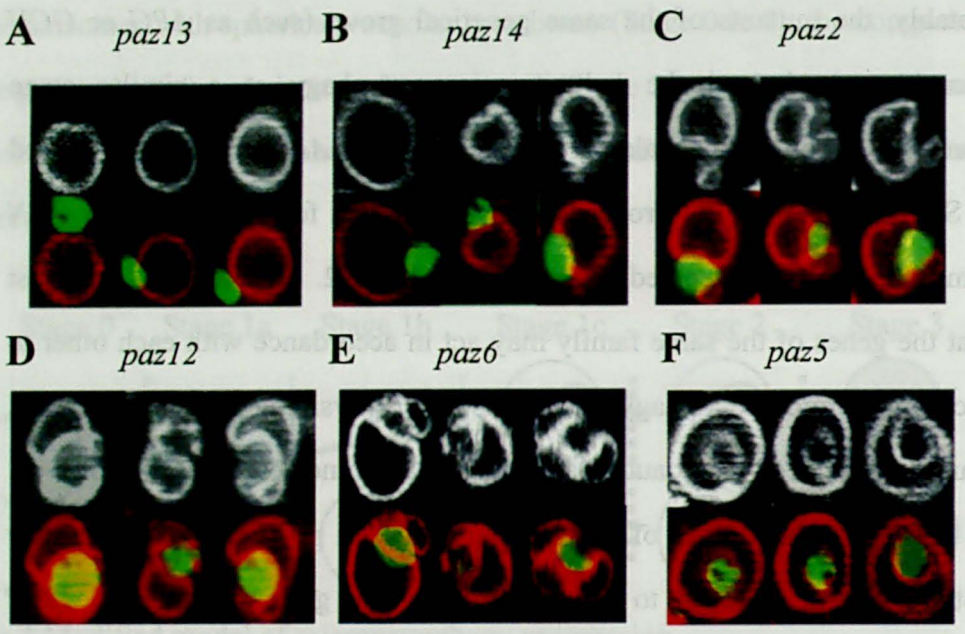

Fig.5 Morphological phenotypes of *paz* mutants.

All *paz* mutants were subjected to fluorescent microscopy 3h after the cells were transferred to SD medium. The representative images were shown in the same manner as Fig.2. (A) *paz13* (*vps15*) cells stopped at Stage 0. (B) *paz14* (*pep4*) stopped at Stage 1a. (C) *paz2* (*apg8*, shown in C) and *paz8* (*apg4*, data not shown) stopped at Stage 1b. (D and E) *paz1* (*apg1*, data not shown), *paz3* (*apg16*, data not shown), *paz4* (*ugt51*, data not shown), *paz6* (YPR049c homologue mutant, shown in E), *paz7* (*apg2*, data not shown), *paz9* (*apg9*, data not shown), and *paz12* (*apg7*, shown in D) stopped at Stage 1c. (F) *paz10* (*gcn1*, data not shown), *paz11* (*gcn2*, data not shown) and *paz5* (*gcn3*, shown in F) stopped at Stage 2.

Discussion

The vacuolar morphological changes until the sequestration of peroxisome were elaborately observed in immobilized cells. The main finding is that vacuolar membrane can form lobe structures along the surface of peroxisome cluster. This phenomenon seems to have some relation to so called vacuolar inheritance *in S.cerevisiae* (5). The process functions to deliver a portion of vacuole into a daughter cell during cell division and contains fission events as well as fusion steps of vacuolar membrane. The small lobes of vacuoles in the inheritance are connected to each other forming tubular structure. The formation of this "segregation structure" was followed by the extension into the bud site along actin cable structures that constitute cell division axis. It is assumed that the molecular mechanism underlying the vacuolar inheritance may also contribute to the lobe formation or its extension along peroxisome cluster during micropexophagy.

The morphological phenotypes of *paz* mutants (Fig.5) indicated the validity of the micropexophagy progression model (Fig.4) composed of several membrane dynamics including vacuolar membrane budding, segregation, fusion, and membrane lysis of peroxisome and vacuolar membrane. The elucidation of molecular complex consisted of the Paz factors in the same group of the morphological test will clarify the actual reactions of each step in micropexophagy.

Summary

By means of time-lapse microscopy of a immobilized cell on the coverslip glass, the author succeeded in chasing the morphological changes of vacuole and peroxisomes during micropexophagy. The observation led to the discovery of a novel mode in the engulfment of peroxisome cluster that undergoes with lobe formation from vacuolar membrane. Based on this result, the schematic model of micropexophagy was reconstructed. The phenotypes of 13 *paz* mutants were investigated morphologically, and classified according to the reconstructed model.

CHAPTER II

Functional analysis of sterol glucosyltransferase Paz4 in pexophagy

SECTION I Analysis of Paz4 and its domain functions in pexophagic processes

Introduction

Pexophagy belongs to cellular degradation systems called autophagy in which vacuole/lysosome plays a central role. In *S.cerevisiae* *APG/AUT* genes are essential for macroautophagy, a bulk degradation pathway of cytosolic components to vacuole under nitrogen-starvation conditions (2, 39, 42), and *CVT* genes are required for constitutive transport of aminopeptidase I (API) to vacuole, the cytosol to vacuole targeting (Cvt) pathway (14, 37). Pexophagy and these pathways share much in their involved genes and thus are thought to use some common molecular machineries (16). The previous study demonstrated that more than 6 *APG* genes had overlapping functions in pexophagy of *P. pastoris* (See Chapter I). One of their acting sites in micropexophagy was a newly-discovered structure, called MIPA (micropexophagic apparatus). The occurrence of MIPA has been revealed by study of another micropexophagy factor Paz2 (Mukaiyama *et al.*, submitted for publication). The formation of MIPA was followed by the homotypic fusion of opposing vacuolar membranes, which was suggested to be coupled with the Paz2-modification pathway, involving Paz8, Paz12, and Gsa20.

Through the mutagenesis method described in Chapter I,

Paz4/Ugt51 (UDP-glucose: sterol glucosyl transferase) was identified as an essential factor in micropexophagy. Interestingly, this gene mutant showed the similar morphological phenotype to the mutants of *APG* homologues, though it *per se* does not belong to *APG* family (Chapter I, Fig.5). Then the author focused on Paz4 to obtain new insights on the specificity of pexophagy as well as the common machinery to other autophagic pathways.

The catalytic activity of Paz4 yields sterol glucoside (SG). Genes encoding for enzymes with the same activity were also cloned from *Saccharomyces cerevisiae* and *Candida albicans* (45), all of which were found to contribute exclusively to SG synthesis with little transfer activities toward other sugars or lipids. SG can act as a "primer" compound for cell wall synthesis in higher plant cell (30) or a certain factor in virulence of phytopathogenic fungus *Colletotrichum gloeosporioides* (21), but the actual role of SG in other organisms are yet to be elucidated.

In addition to the catalytic domain at its carboxyl terminal region, Paz4 has two other motifs in its amino terminal region: pleckstrin homology (PH) domain and GRAM domain. GRAM domain was named after four representative proteins: glucosyltransferases, Rab-like GTPase activators, and myotubularins (8, 48). It consists of about 70 amino acid residues and is predicted to form four beta-strands and one alpha helix. Proteins harboring the GRAM domain exist widely in eukaryotes, many of which are assumed to be putative membrane proteins. However, this domain's physiological and biochemical function is not known except that some patients of X-linked myotublar myopathy harbor the amino acid substitutions within the GRAM domain of human myotubularin gene (7, 22).

The author investigated the role of GRAM domain as well as other domains in Paz4, and this work is the first report of GRAM domain function.

Materials and methods

Strains and media

The strains used in this study are listed in table I. For growing yeast cells in rich medium the author used YPD (1% yeast extract, 2% peptone, and 2% glucose) or SD (0.67% yeast nitrogen base without amino acid (YNB), 2% glucose and auxotrophic amino acids if necessary). Peroxisome induction was done in SM (0.67% YNB, 0.5% methanol and auxotrophic amino acids), and subsequent pexophagy induction was made by the medium shift to SD (micropexophagy) or SE (0.67% YNB, 0.5% ethanol and auxotrophic amino acids) (macropexophagy). For assaying macroautophagy competence, the author transferred the cells to SD (-N) (0.17% YNB without amino acids and nitrogen, and 2% glucose). All the composites used in these media were purchased from Difco.

DNA manipulation

***PAZ4* disruption**: The construct for *PAZ4/ UGT51B1* (GenBank™ accession number AF091397) disruption was a kind gift from Dr. Warnecke (University of Hamburg, Germany), which contains the *Sh ble* gene flanked by 0.5kb stretches homologous to the *UGT51B1* 3'- and 5'-noncoding region. This plasmid (pGZTP) was digested by *Eco* RI /*Eco* RV and

introduced into *P.pastoris* strain PPY12. The correct replacement of *UGT51B1* was confirmed by Southern Blot analysis and the selected strain was designated PZO101.

Construction for GFP-Paz4 expression: The *PAZ4* ORF was amplified with the primers designated NhePaz4u and Paz4d (Table 2), which was cloned into the pGEM-T vector (Invitrogen) resulting in pPAZ41. *GFP* sequence was PCR-amplified with pTW51 (33) as template and the primers BamGFP5 and GFP3Nhe (Table 2), which was then cloned into the pGEM-T vector resulting in pGFP1. The sequence containing GFP-coding region was excised from pGFP1 with *Spe* I/*Nhe* I and cloned into *Spe* I/ *Nhe* I-treated pPAZ41, which gave pGPZ41 construct. The fragment containing GFP and 3.0kb region of Paz4 ORF was excised from pGPZ41 with *Bam* HI and was ligated with the *Bam* HI-fragment from pC3.5-1, a plasmid with *PAZ4* ORF and *P.pastoris HIS4* generously provided by Dr. Warnecke. The resultant plasmid (pGPZ42) was digested with *Stu* I and introduced into strain PZO101 (strain PZO201). The entire sequence of *GFP-PAZ4* ORF in pGPZ41 was also cut out with *Spe* I/ *Sac* I and cloned into pHM100 (26) derivative plasmid to which *PAZ4* 5'-noncoding region had been cloned .The resultant plasmid pGPZ43 was digested with *Stu* I and introduced into strain PZO101 (Strain PZO200).

Construction of Paz4 derivatives with domain-deletion or point mutation: In order to generate PH or GRAM domain mutation, the author used QuikChange™ Site-Directed Mutagenesis Kit (Strategene) that applies inverse PCR method with pGPZ42 as template. The author deleted or mutated following amino acid residues of Paz4: the region from a.a.248 to

a.a 349 eliminated as PH domain deletion (with primers PHfw and PHrv, see Table II for the actual DNA sequences), from a.a. 588 to a.a 652 as GRAM domain deletion (with primers GRAMfw and GRAMrv,), and the substitution of tyrosine residue at a.a. 642 to proline for point-mutation inside GRAM domain (with primers Y642Pfw and Y642Prv). The resulting plasmid constructs were named according to the mutation introduced: pGPZ4dPH (PH domain deletion), pGPZ4dGRAM (GRAM domain deletion), and pGPZ4Y642P (amino acid replacement within GRAM domain). For expression of GFP-Paz4 truncated at amino acid 765 of Paz4 ORF, the corresponding fragment was PCR-amplified with primers BamGFP5 and Paz4tr765 (Table 2), and the amplified fragment was digested with *Bam* HI and cloned into *Bam* HI/ *Sna* BI-treated pPIC3K vector (Invitrogen) to generate pGPZ4dCT. All the three plasmid were linearized with *Stu* I, and introduced into strain PZO101. The construct which contains PH domain deleted PAZ4 ORF under its own promoter regulation was the ligation product of *Aat* II/ *Not* I cleaved pGPZ4dPH and pEAE.

Alcohol oxidase (AOD) –degradation assay and immunoblot analysis

The active staining of AOD was performed as AOD assay for micropexophagy competence. The AOD assay for macropexophagy was a modified method of that for micropexophagy in that the AOD degradation was induced on SE plate and the SE shift was prolonged to 48h. Immunoblot analysis of AOD degradation was done as described previously (26).

Lipid extraction and analysis

Lipid extraction and analysis were performed as described previously (45).

Alkaline phosphatase assay

A plasmid pTN3, which contains the truncated form of S.cerevisiae PHO8 gene (28), was introduced into strains BY4741 (wild type), ugt51, and GSY1 (*apg1*). The cells at log-phase were transferred to SD (-N) and incubated for 4.5h. The alkaline phosphatase activity of each strain was determined as described elsewhere (28).

API processing detection

Wild type strain (BY4741), ugt51, and GSY1 (*apg1*) were grown in 0.17% YNB, 0.5% ammonium sulfate, 0.5% casamino acid, and 2% glucose. The cells at log-phase were harvested and disrupted with alkaline method (27). Total cell lysate was subjected to immunoblot analysis with anti-API antibody in the same way as described previously (19).

Cell viability test

The cells were first grown on YPD to a stationary phase and subsequently transferred to SD (-N) medium at OD_{610}=0.1. The culture was incubated with vigorous shaking at 28 °C for 7 or 10 days, and the diluted culture was plated on YPD plate. The colony number formed after 2-day incubation was counted which we referred to as cell viability value.

Observation of macroautophagic bodies

The observation of macroautophagic bodies is performed as described previously (39).

Fluorescence microscopy

The observation of peroxisome-vacuole dynamics was done as described previously (33). To visualize the localization of GFP-Paz4 or its derivatives, cells were labeled with 0.93μg/ml FM4-64 (Molecular Probes) during 12 h-incubation in SM medium with starting OD at 0.5. Then the cells were shifted to SD or SE medium and were subjected to observation with IX70 fluorescence microscope (Olympus). Images are acquired with a Sensys™ CCD (Charged Coupled Device) camera (Photometrics) and analyzed on MetaMorph imaging software (Universal Imaging Corporation).

Table 1. Yeast strains used in this study

Strain	Genotype	Reference
P. pastoris		
PPY12	*arg4 his4* (parental strain for *PAZ41* deletion)	Sakai et al. 1998
STW1	PPY12 *his4*::P_{AOX1}*GFP*-PTS1-*HIS4* (GFP targeted to peroxisomes.)	Sakai et al., 1998
PZR7	STW1 *paz7*::*Zeocin*^{R}	Mukaiyama et al., 2002
PZR12	STW1 *paz12*::*Zeocin*^{R}	Mukaiyama et al., 2002
PPM5015	PPM5010 *his4*::pHM108 (P_{PAZ2}*GFP-PAZ2* HIS4)	Mukaiyama et al., 2002
PZO101	PPY12 *ugt51*::*Zeocin*^{R} (*PAZ4*-deleted strain)	this study
PZO102	PZO101 *his4*::P_{UGT51}*PAZ4-HIS4* (pEAE)	this study
PZO103	PZO101 *his4*::P_{AOX1}*GFP*-PTS1-*HIS4* (pTW51)	this study
PZO104	SMD1163 (*pep4 prb1 his4*) *his4*::pTW51 *ugt51*::Zeocin	this study
PZO105	PZO101 *his4*::P_{UGT5}*PAZ4*-PHΔ (pPZ4dPH)	this study
PZO200	PZO101 *his4*::P_{UGT51}*GFP-PAZ4 -HIS4* (pGPZ43)	this study
PZO201	PZO101 *his4*::P_{AOX1}*GFP-PAZ4 -HIS4* (pGPZ42)	this study
PZO202	PZO101 *his4*::P_{AOX1}*GFP-PAZ4* -PHΔ-*HIS4* (pGPZ4dPH)	this study
PZO203	PZO101 *his4*::P_{AOX1}*GFP-PAZ4* -GRAMΔ-*HIS4* (pGPZ4dGRAM)	this study
PZO204	PZO101 *his4*::P_{AOX1}*GFP-PAZ41*-CATΔ-*HIS4* (pGPZ4dCT)	this study
PZO205	PZO101 *his4*::P_{AOX1}*GFP-PAZ4*-Y642P-*HIS4* (pGPZ4Y642P)	this study
PZO302	PZO101 *his4*::pHM108	this study
S. cerevisiae		
BY4741	MATa *his3 leu2 met15 ura3* (parental strain for *UGT51* deletion)	Suzuki et al., 2001
GSO1	BY4741 *ugt51*::*Kanamycin*^{R}	this study
GSY102	SEY6210 *apg1*::*LEU2*	Suzuki et al., 2001

Table 2 Oligonucleotide primers used in this study

Primer name	DNA sequence
NhePaz4u	CTAGCTAGCTCACAACTCAGACCCAGAGAT
Paz4d	CGAGCTCGCTTATTTGGCACCAGTACTTG
BamGFP5	CGGGATCCATGAGTAAAGGAGAAGAACTTTTT
GFP3Nhe	CTAGCTAGCTTTGTATAGTTCATCCATGCCAT
PHfw	TTTCTTCCGAAAAGAGACTCCACTAAGAATAGCGGTGGTCATGTCACC
PHrv	GGTGACATGACCACCGCTATTCTTAGTGGAGTCTCTTTTCGGAAGAAATG
GRAMfw	GAAAGAGAAGTTGCACAGTCCAGAGGCTTTAGATTCGGGTACTCTGGG
GRAMrv	CCCAGAGTACCCGAATCTAAAGCCTCTGGACTGTGCAACTTCTCTTTC
Y642Pfw	ATTATAAACATTCTCAATATCGGAAGGTGGAAGTATCATAGTTGTGTTTCTG
Y642Prv	CACAAACACAACTATGATACTTCCACCTTCCGATATTGAGAATGTTTATAAT
Paz4tr765	GAGGAGGTACAAATTTGTGCTATAAATCGATGG

Results

Paz4 is required for micropexophagy and macropexophagy.

The *PAZ4*-encoding ORF was deleted from the *Pichia pastoris* genome. The derived *paz4* null mutant strain PZO101 and the wild type strain were subjected to alcohol oxidase (AOD)-degradation assay (Materials and Methods), which visualizes the remaining activity of peroxisome matrix protein alcohol oxidase as a quantitative index of non-degraded peroxisomes. As shown in Fig.1A, after the AOD-degradation assay, the *paz4* null mutant exhibited deep-purple colonies after adaptation to both micropexophagy (after shift to the synthetic dextrose (SD) medium) and macropexophagy (after shift to the synthetic ethanol (SE) medium). In contrast, colonies of the wild type strain PPY12 remained white. The ability to degrade AOD in *paz4* null mutant was

recovered by introducing the *PAZ4* gene into strain PZO101. The defect of AOD degradation in strain PZO101 was also confirmed by immunoblot analysis using anti-AOD antibody (Fig.1B). The 78-kD band cross-reactive with AOD disappeared 9h after the SD shift in strain PPY12, but it remained in *paz4* null mutant. Taken together with the results from fluorescent analyses shown below (Fig.3), the author concluded that the *PAZ4* was essential for both micropexophagy and macropexophagy.

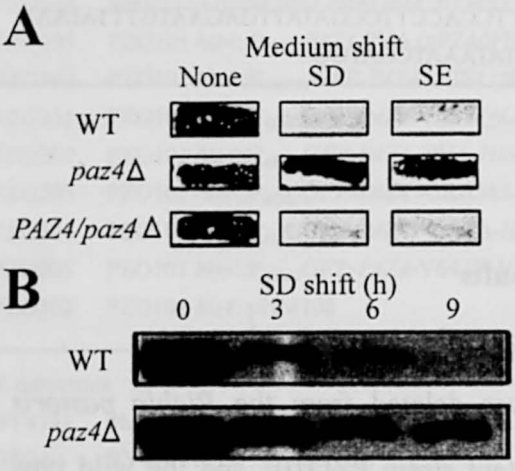

Fig.1 Pexophagy defects in *PAZ4* disruptant.
(A) AOD assay for wild type strain (WT, strain PPY12), *PAZ4* disruptant (*paz4*Δ, strain PZO101), and *PAZ4*-complemented strain (PAZ4/ *paz4*Δ, strain PZO200) was done. In the *paz4*Δ strain AOD activity remained both after SD and SE shift of the carbon source.
(B) The persistent AOD amount was estimated by immunoblot analysis. The *paz4*Δcells had non-degraded AOD even 9h after the carbon source shift to SD.

Since the *PAZ4* encodes ergosterol glucosyl transferase, the amount of the reaction product SG was compared between the wild type and *PAZ4*-disrupted strain PZO101. As expected, SG could not be detected in strain PZO101 (Fig.2) indicating that Paz4 is the solo or main enzyme responsible for SG synthesis in *P. pastoris*. Next, SG and its derivatives were tested for their ability to complement the pexophagy defect of *paz4*

null mutant. However, various trials were unsuccessful. In addition, the total amount of SG in the *P. pastoris* wild type cells did not change significantly between before and after the pexophagy (data not shown). Then we concluded that the bulk existence of SG is not sufficient for micropexophagy accomplishment.

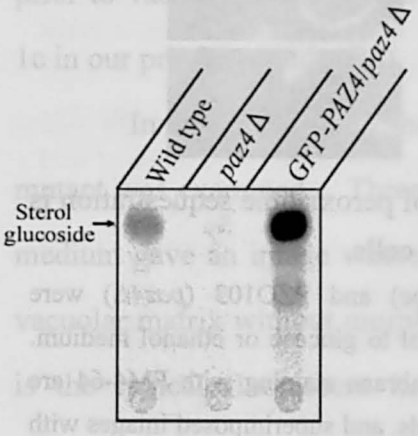

Fig.2 Thin layer chromatography of *PAZ4*-disruptant.
Total lipid was retrieved for the strains listed and was subjected to thin layer chromatography. The spots for SG were shown. The *paz4*Δ strain had no visible mount of SG.

Characterization of pexophagy in the *paz4* null mutant using fluorescent-labeled cells.

We adopted to *paz4* null mutant a previously developed fluorescent method to determine at which stage the *paz* mutant strain ceased during micropexophagy (33). When the cells were shifted to the SD medium to induce micropexophagy for 3 h, the strain PZO103 had deeply invaginated vacuoles wrapping the peroxisomes (Fig.3A). The opposite tips of the vacuolar membrane extension often kept contact with each other, but the boundary never disappeared at any time point during the observation.

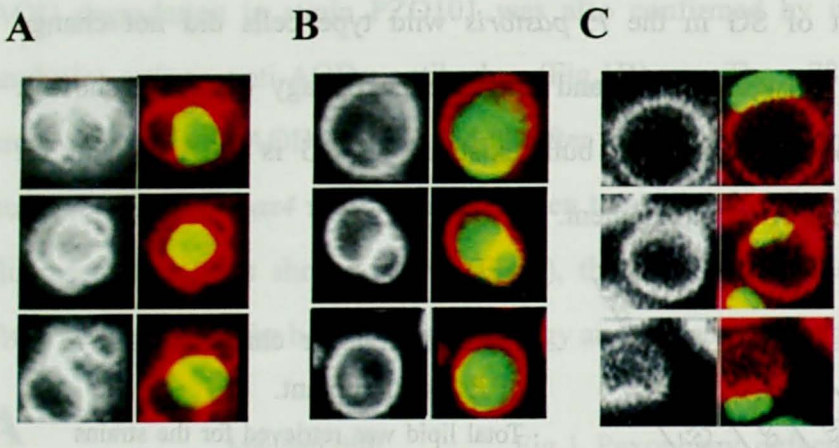

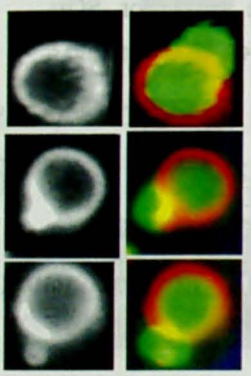

Fig.3 The final stage of peroxisome sequestration is inhibited in the *paz4*Δ cells.

Strain STW1 (wild type) and PZO103 (*paz4*Δ) were transferred from methanol to glucose or ethanol medium. Images of vacuolar membrane staining with FM4-64 are presented in the left panels, and superimposed images with FM4-64 (red) and GFP-PTS1 signal (peroxisomal matrix, green) are shown in the right panels. (A) In *paz4*Δ cells, deeply invaginated vacuoles enwrapping intact peroxisomes were observed following 3 h incubation in glucose medium, but the GFP signal never diffused throughout the vacuole. (B and D) In the wild-type strain, GFP-fluorescence appeared diffusely throughout the vacuolar lumen 3 h after transfer to glucose (B) or ethanol medium (D) indicating normal procession of pexophagy. (C) The morphology of vacuole and peroxisome did not change for 3 h after transfer of *paz4*Δ cells from methanol to ethanol.

Wild type cells (strain STW1) showed all the steps of vacuolar dynamics during micropexophagic process including Stage 2 cells where the GFP-PTS1 fluorescence was diffused in a vacuole matrix (Fig.3C). From these results the author assumed that the *paz4* mutant has certain impairments in the homotypic fusion of vacuolar membrane or reactions just prior to vacuolar fusion event during micropexophagy, designated as Stage 1c in our previous study (26).

In a similar way, the macropexophagic defect in the *paz4* null mutant was examined. Three-hour incubation of wild type cells in the SE medium gave an image where GFP-PTS1 fluorescence was diffused into a vacuolar matrix without morphological changes of vacuole (Fig.3D). This is the typical fluorescent image for macropexophagy (33). However, GFP-PTS1 fluorescence remained intact in strain PZO103 after SE shift for 3 h (Fig.3C). These microscopic observation results were consistent with those from AOD assay (Fig.1), confirming that *paz4* null mutant is not capable of both micro- and macro-pexophagy.

PAZ4 is not necessary for both starvation-induced macroautophagy and Cvt pathway.

To test the involvement of Paz4 in nitrogen starvation-induced macroautophagy in *P. pastoris*, light-microscopic observation of the macroautophagic bodies was made as described. (39). The addition of 1mM phenylmethylsulfonyl fluoride (PMSF) to the SD medium without nitrogen resource, SD (-N), and further incubation of *Pichia* cells for 8 h gave one or two black dots in vacuole matrix of wild-type cells as well as in

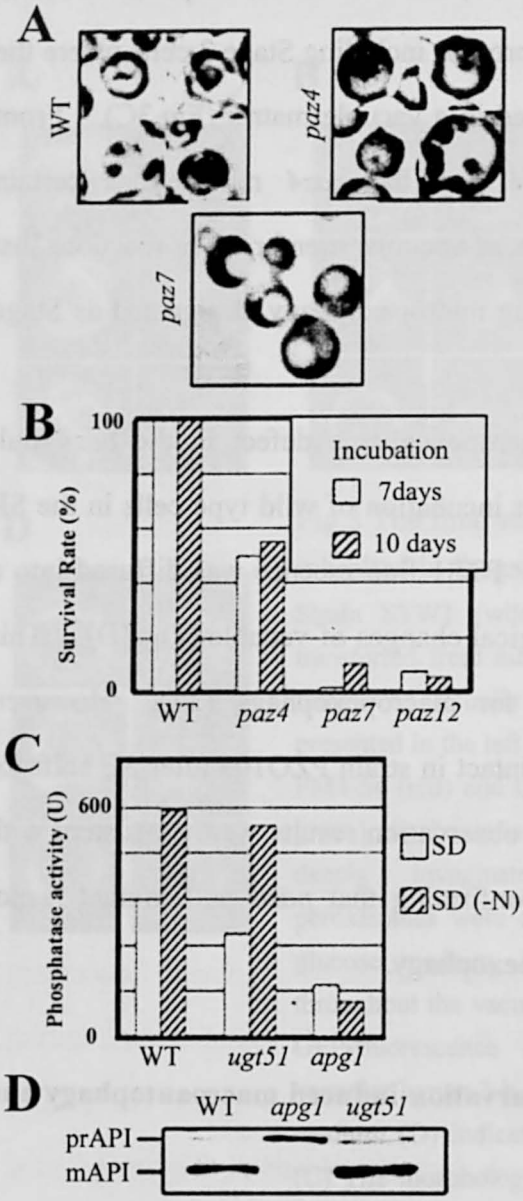

Fig.4 *PAZ4* and its counterpart in *S.cerevisiae* are not involved in macroautophagy nor Cvt pathway.

(A) The light microscopy of the wild type strain PPY12, *paz4*Δ strain PZO101, and *paz7* strain PZR7 cells was done after 8h incubation in SD (-N). In WT and *paz4* cell, a black dot structure was visible in the bright part of vacuolar lumen. (B) The colony formation competence of wild type strain PPY12 (WT) and other micropexophagy mutants was measured after 7days (open) or10 days (striped) incubation in SD (-N). The results were presented in percentage so that the colony formation ability for strain PPY12 was 100%. (C) *S. cerevisiae* strains harbouring the truncated form of Pho8 were cultured in SD (open) or SD (-N) (striped), and the phosphatase activity of processed Pho8 in each cell lysate was determined. The value (phosphatase activity) was standardized with the protein concentration of each sample. The *ugt51* strain had the enzyme activity indistinguishable from that of wild type cells.

that of *PAZ4*-disrupted strain PZO101 (Fig.4A). In contrast, no such grains were found in *paz7* mutant strain PZR7 (*S. cerevisiae APG2* homologue mutant), indicating that *paz4* null mutant still underwent normal transport of autophagosome into vacuole.

The intactness of macroautophagy in *paz4* was also supported by the following viability test. Macroautophagy impairment halts cellular protein turnover which leads to reduced viability in nitrogen-limited media (42). After 7 or 10 day incubation in SD (-N) medium, *paz4* null mutant (strain PZO101) retained substantial survival rate approximately half of that of wild type cells (Fig.4B). On the other hand, the same treatment greatly diminished the viability of the *paz7* (*Pichia apg2* mutant) and *paz12* mutant (*Pichia apg7* mutant) (Fig.4B).

The *PAZ4/UGT51* (YLR189c) is the only ortholog of *PAZ4* in *S. cerevisiae*. Next, the involvement of *UGT51* in macroautophagy and the Cvt pathway transport was studied in *S. cerevisiae*. The ability of macroautophagy was assessed by alkaline phosphatase assay (28). In this experiment the enzymatic activity from vacuole-transported and matured alkaline phosphatase was determined as a measure of macroautophagy completion. In *ugt51* strain GSO1, the phosphatase activity was enhanced up to nearly 2 folds when the cells were incubated in the SD (-N) (Fig.4C), almost the same level as that in wild type strain (BY4741). In contrast *apg1* (strain GSY102) showed no augmentation in the phosphatase activity in SD (-N) medium (Fig.4C).

The intactness of Cvt pathway was also tested by visualizing the API forms in each cell lysate (19). In *paz4*, both processed and

unprocessed band were detected by immunoblot analysis (Fig. 4D). The band pattern was identical to the results with wild-type strain. The cell-free extract from *apg1* strain contained no detectable band for the processed form.

These results altogether show that the deletion of the orthologue gene to *PAZ4* did not cause any detectable defects in macroautophagy nor Cvt pathway in *S.cerevisiae*. Notably, among known *PAZ/ GSA* genes, the *PAZ4* is the only gene essential for both micro- and macropexophagy, which were not involved in macroautophagy or in the Cvt pathway.

GRAM and catalytic domain of Paz4 are essential for micropexophagy.

To study further on the role of Paz4 and SG synthesis in pexophagy, the author constructed green fluorescent protein (GFP)-tagged Paz4 (GFP-Paz4) proteins lacking one of PH-, GRAM-, and catalytic domains, yielding GFP-Paz4dPH, GFP-Paz4dGR, GFP-Paz4dCT, respectively (Fig.5B). The role of each domain on Paz4 in micropexophagy was assessed by the AOD-degradation assay.

GFP-Paz4 derivatives without GRAM domain (GFP-Paz4dGRAM) or catalytic domain (GFP-Paz4dCT) could not rescue the impairment of micropexophagy in strain PZO101, even though these proteins are expressed abundantly under *AOX1* promoter (Fig.5B). These show that both catalytic and GRAM domains are indispensable for Paz4 function in micropexophagy. The Paz4 constructs lacking PH domain brought partial complementing effects on micropexophagy (Fig.5B).

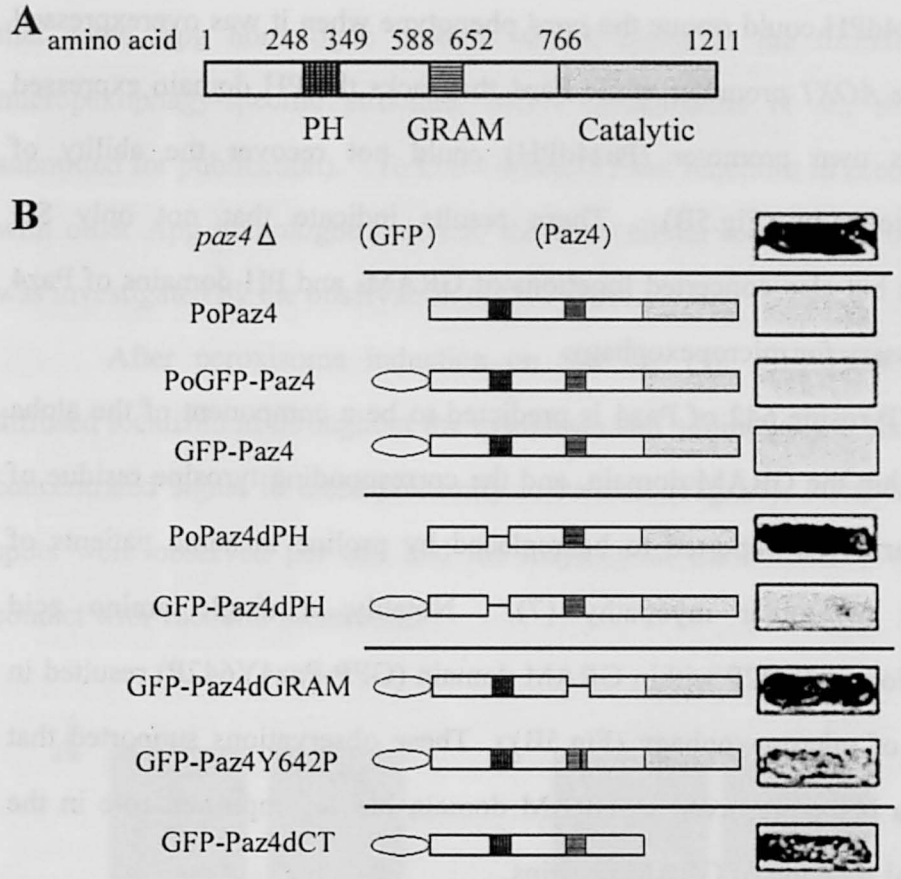

Fig.5 Functional domains of the sterol glucosyltransferase Paz4.

(A) Schematic drawing of the annotated domains withinPaz4.

(B) Various Paz4 variants were expressed in *paz4*Δ cells. Po means the expression under *PAZ4* original promoter. Their expression products are depicted in the middle. Persistence of Aox is shown on the right panel. The strains with GRAM or catalytic domain-mutated Paz4 retain Aox activity (strain GFP-Paz4dGRAM, GFP-Paz4Y642P, and GFP-Paz4dCT). The PH domain deletion displayed impaired pexophagy when the enzyme was expressed under its original promoter (strain PoPaz4dPH), but not when it was expressed under the *AOX1* promoter (strain GFP-Paz4dPH).

GFP-Paz4dPH could rescue the *paz4* phenotype when it was overexpressed under the *AOX1* promoter while Paz4 that lacks the PH domain expressed under its own promoter (Paz4dPH) could not recover the ability of micropexophagy (Fig.5B). These results indicate that not only SG synthesis but also concerted functions of GRAM- and PH-domains of Paz4 are necessary for micropexophagy.

Tyrosine 642 of Paz4 is predicted to be a component of the alpha helix within the GRAM domain, and the corresponding tyrosine residue of myotublarin was reported to be replaced by proline in some patients of X-linked myotublar myopathy (7). Notably, a single amino acid substitution of Y642P within GRAM domain (GFP-Paz4Y642P) resulted in the loss of micropexophagy (Fig.5B). These observations supported that the alpha helix preserved in GRAM domain has an important role in the biological function of GRAM proteins.

Localization of Paz4 during micropexophagy depended on GRAM domain.

Although Paz4 was found to be dispensable for other autophagic pathways, several results suggest that this gene product may function in collaboration with other Apg/Aut or Cvt homologue proteins. First, *PAZ4* disruption inhibited both micro- and macro-pexophagy (Fig.1), which was the same phenotype as that of the homologue mutants (50). Secondly, the organelle morphology of *paz4 null* mutant showed that it ceased the micropexophagic process just before vacuolar homotypic fusion, the very step at which the homologue mutants halts (26). Our recent work found

that some Apg homologue proteins are involved in the formation of micropexophagy-specific structure, MIPA (Mukaiyama et al., subscript submitted for publication). To know whether Paz4 functions in accordance with other Apg homologue proteins, the intracellular localization of Paz4 was investigated by the observation of GFP-Paz4.

After peroxisome induction on SM for 15h, GFP-Paz4 had a diffused localization throughout the cytoplasm and additionally it showed a concentrated signal in close proximity to vacuole (Fig.6A). One to three spots were observed per cell and the majority of the structures were in contact with vacuolar membrane.

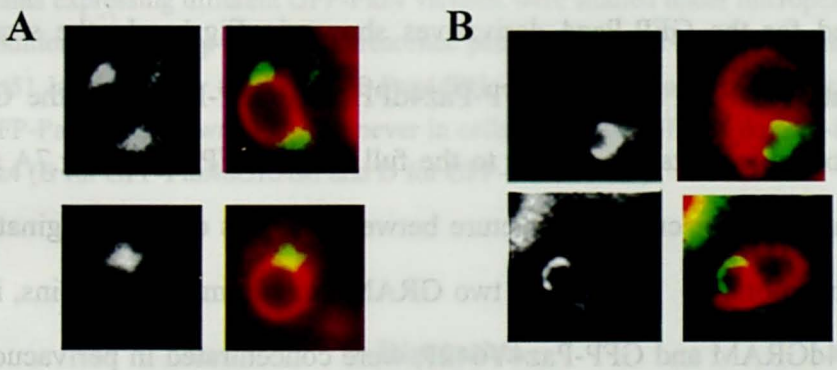

Fig.6 GFP-Paz4 localization pattern changes during micropexophagy.
(A) Strain PZO202 was grown on SM for 15h and the fluorescence images from FM4-64 and GFP-Paz4 were acquired (left panels). The two signals were merged (red: FM4-64, green GFP-Paz4) whose images were presented on the right panels. GFP-Paz4 signal was concentrated in proximity to vacuolar membrane. (B) The same strain shown in (A) was shifted from SM to SD medium and incubated for 90min. The acquired images were shown in the same way as (A). The GFP signal pattern changed into a cup-shaped structure.

Subsequent shift of the cells to SD showed a gradual change in GFP-Paz4 distribution. The fraction of cells with the spot structure came to decrease and instead a cup-shaped pattern appeared, and 90min incubation resulted in the perfect disappearance of the spot pattern (Fig.6B). The observed structure was mostly in contact with invaginating vacuolar membrane at both tips. The observed localization of GFP-Paz4 had a strong similarity to that of GFP-Paz2, which is attached to MIPA (26). Indeed, in *paz4* null mutants expressed GFP-Paz2 never formed the cup-shaped pattern which is apparent in *paz2* cells (data not shown). Thus the author assume that Paz4 may be localized to MIPA.

Finally, association of Paz4 with cup-like structure (possibly MIPA) was tested for the GFP-Paz4 derivatives shown in Fig.1. In the strains having intact GRAM domain, GFP-Paz4dPH and GFP-Paz4dCT, the GFP signal showed localization similar to the full length GFP-Paz4 (Fig.7A and 7C). They had the cup-like structure between the tips of the invaginating vacuolar membrane. In contrast, two GRAM domain mutant proteins, i.e., GFP-Paz4dGRAM and GFP-Paz4Y642P, were concentrated in perivacuolar region, but never formed the cup -like structure (Fig.7B and 7D). Therefore, the author concluded that the association of Paz4 to MIPA-like structure depended on GRAM motif. This result also confirmed the important role of the tyrosine residue (Y642) within the GRAM domain in the intact function of the whole domain.

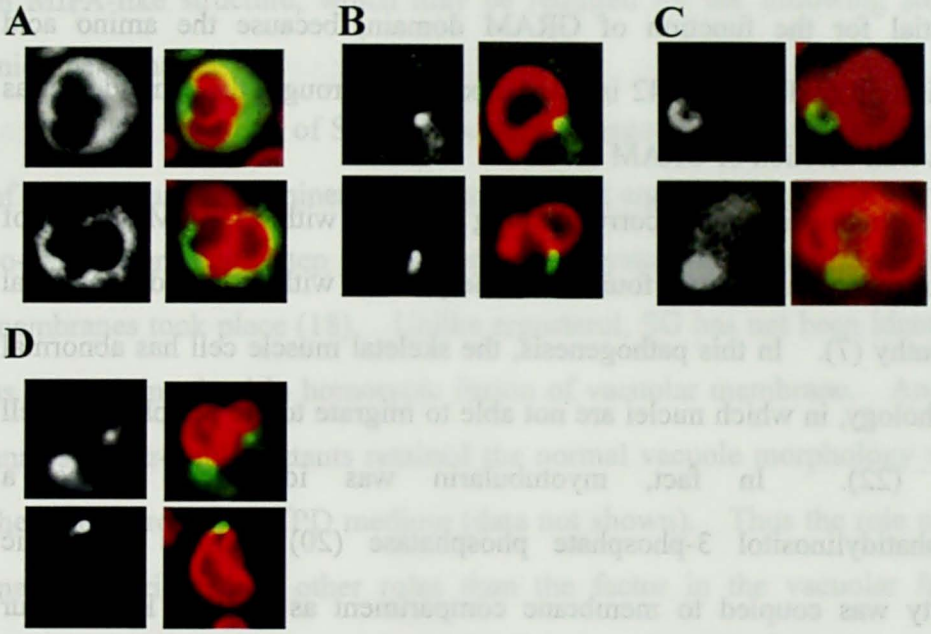

Fig.7 Localization patterns of GFP-Paz4 mutated in each domain.
Strains expressing different GFP-Paz4 variants were studied under micropexophagic conditions. The cup-shaped fluorescence pattern was observed in cells expressing Ugt51 lacking either the PH (GFP-Paz4dPH, shown in A) or the catalytic domain (GFP-Paz4dCT, shown in C), but never in cells expressing GRAM domain-impaired Paz4 (B for GFP-Paz4dGRAM and D for GFP-Paz4Y642P).

Discussion

GRAM domain can be a membrane localization motif.

A computational analysis predicted the existence of GRAM motif (8). The members with GRAM domain range from yeast to human proteins. Although the amino acid sequences within GRAM domain are not highly conserved (for instance, human myotubularin-like proteins gives similarity to the yeast glucosyltransferases at E=1.4), they are predicted to share some structural feature: they contain four beta strands followed by one alpha helix. Our results showed that the alpha helix composition was

essential for the function of GRAM domain, because the amino acid substitution of Tyrosine 642 in this helix region brought the same defect as the overall deletion of GRAM domain.

Interestingly, the corresponding mutation within GRAM domain of human myotubularin was found in some patients with X-linked congenital myopathy (7). In this pathogenesis, the skeletal muscle cell has abnormal morphology, in which nuclei are not able to migrate to the periphery of cell body (22). In fact, myotubularin was identified to be a phosphatidylinositol 3-phosphate phosphatase (20) and its enzymatic activity was coupled to membrane compartment as well as Paz4. Our observation indicated that GRAM domain is responsible for the MIPA-like structure localization of the host protein, which suggests that the same motif may act as a localization determinant as for myotubularin.

Deduced function of ergosterol glucoside (SG).

The catalytic region-deleted GFP-Paz4 was not functional in micropexophagy (Fig.5B). Interestingly, this variant was able to be localized to MIPA-like structure (Fig.7C). Thus the catalytic activity of Paz4 is not necessary for its localization but essential for its function in micropexophagy. This result has some consistency with that from the lipid experiments in this study: The overall lipid content did not change during micropexophagy (data not shown), and a GFP-Paz4 variants (GFP-Paz4dGRAM), which had been turned out to be capable of SG synthesis, could not recover the *paz4* defect (Fig.5B). These results altogether imply that the enzyme localization may ensure SG concentration

in MIPA-like structure, which may be required for the following step in micropexophagy.

The lipid part of SG in *P. pastoris* is ergosterol. An *in vitro* assay of vacuole fusion machinery demonstrated that ergosterol was necessary for so-called "priming" step just before the physical contact of the facing membranes took place (18). Unlike ergosterol, SG has not been identified as a factor involved in homotypic fusion of vacuolar membrane. And the analysed *paz4*-null mutants retained the normal vacuole morphology when they were grown on YPD medium (data not shown). Thus the role of SG may be attributed to other roles than the factor in the vacuolar fusion process. Yet there is much possibility that the SG formation or the modification of ergosterol can regulate the timing of vacuolar fusion events. The precise role of this glycolipid awaits further study.

The specificity of Paz4 action on pexophagy.

Our previous study identified 14 genes involved in micropexophagy. Most of these *PAZ* members have their counterparts in *S.cerevisiae* that are found to function in macroautophagy or Cvt pathway (26). In contrast *PAZ4* is quite unique in that it does not belong to the *APG/AUT* nor *CVT* family, while it is essential for both modes of pexophagy (micro- and macro-pexophagy) (Fig.1 and 3).

The specificity of Paz4 contribution to pexophagy processes suggests one possibility that this molecule may function in peroxisome recognizing reaction. In macropexophagy, the *de novo* formation of autophagosome-like structure occurred along with peroxisome cluster

resulting in macropexophagosome (43). Similarly, MIPA partially extends to the surface of peroxisome cluster during micropexophagy (Mukaiyama *et al.,* submitted for publication). Since Paz4 is localized in MIPA-like structure, it could interact with peroxisomal membrane partner to capture the organella. Further localization study of Paz4 using the domain-mutated derivatives will be of great importance to elucidate the specific action of Paz4 as well as the peroxisome-targeting machinery of pexophagy in general.

SECTION II Biochemical assay for the lipid binding ability of GRAM domain in Paz4

Introduction

In the last section, the author found the essential role of GRAM domain of Paz4 protein. Especially it was found to be important for the recruitment of the host protein to a certain subcellular structure, possibly MIPA. Even the replacement of one amino acid residue (Tyrosine 642) in the domain caused the defect in micropexophagy, suggesting that the proper folding of the domain may be required for its function.

Domains required for protein localization are known to interact with some factors such as other protein domains or some specific lipids(6, 23, 49). Many of identified GRAM domains coexist in the host proteins with other domains for membrane binding, such as PH (Paz4), FYVE (*C. elegance* glucosyltransferase), and TBC domain (putative Rab-like GTPase activators). This fact gives rise to one possibility that GRAM domain may be also a membrane-binding domain which acts co-ordinately with the accompanying domain to determine the precise localization of the host protein. Thus the author examined the binding ability of the GRAM domain to various phospholipids, especially the derivatives of phosphatidyl inositol. This study lead to the finding of the interaction between the GRAM domain of Paz4 and phosphatidyl inositol 4'-monophosphate. The significance of the binding property will be discussed in this section.

Materials and methods

Expression of GST (glutathion-S-transferase)- and YFP (Yellow Fluorescent Protein)-tagged GRAM domain in *E. coli*

The DNA encoding YFP is a kind gift from Dr. Noda (National Institute for Basic Biology, Okazaki) and cloned into pHM100 with the 5'-end linked to *Bam* HI site and the 3'- end linked to *Spe* I site. The GRAM domain of Paz4 was PCR amplified with the primers GRAM-N-Nhe (CTGAGCTAGCGTGACCATGTATGGTGCCTTG) and GRAM-C-Xho (CCGCTCGAGTTACTTCAAATTATAAACATTCTCAAT). The amplified fragment was treated with *Nhe* I/ *Xho* I and ligated into the YFP-containing pHM100 cleaved with *Spe* I/ *Xho* I. The resultant YFP-GRAM part was cut out with *Bam* HI/ *Xho* I and cloned into pGEX6P-1 (Amersham) treated with *Bam* HI/ *Xho* I, which gave pGST-YFP-GRAM. This plasmid was introduced to *E. coli* strain BL21 DE3 Rosetta (Gibco). Ampicillin- and Chloramphenicol-resistant colony was chosen, grown on LB at 33 °C to an O.D. unit of 2.0. IPTG (isopropyl β-D-thiogalactopyranoside) was then added at 2mM concentration. The cells were further incubated at 25 °C for 8h to induce the protein expression.

Partial purification of GST- and YFP-tagged GRAM domain

The cells expressing the tagged GRAM domain was retrieved, washed in PBS (137 mM NaCl, 26 mM KCl, 10 mM Na_2HPO_4, and 18 mM KH_2PO_4, pH 7.4) and French-pressed in PBS containing 100 μg/ml APMSF (4-amidinophenylmethansulfonyl fluoride). The suspension was centrifuged at 1,000 × *g* for 10min, and the supernatant fraction was mixed

with Triton X-100 (final concentration: 0.1% v/v). The mixture was further centrifuged at 1,000×*g* for 10min and the supernatant fraction was mixed with 1.5 ml of Glutathione Sepharose 4B resin (Amersham) for 3h at 4°C. After the resin was washed 3 times with PBS, the bound protein was eluted with 10mM glutathion (reduced form) solution in 25 mM Tris, pH 8.0 containing 0.1% v/v Triton X-100. The elutant was subjected to dialysis in PBS.

PIP-Strips™ assay

PIP-Strip™ (Echelon) was soaked in TBS-T buffer (137 mM NaCl, 26 mM KCl, 25 mM Tris and 0.05% v/v Tween-20, pH 7.6) containing 3% w/v fatty acid-free BSA(bovine serum albumin, Wako) and incubated for 1h. The membrane was incubated with the purified protein at 0.6 μg/ml concentration in TBS-T buffer at 4 °C for 12h. After rinsed with TBS-T buffer, it was incubated with 2,000 time-diluted Goat anti-GST antibody (Amersham) in TBS-T containing 3% fatty acid-free BSA for 1h at room temperature. The membrane was rinsed with TBS-T buffer and incubated with 10,000 time-diluted anti-goat IgG antibody in TBS-T buffer for 1h at room temperature. The signal was visualized through ECL (enhanced chemiluminescence) detection kit (Amersham).

Liposome binding assay

The liposome preparation method was the modification of that described by Burd and Emr (3). The 1:1 molar ratio of PS (phosphatidyl L-serine) and PI (phosphatidyl inositol) solution (Both from Sigma) was

mixed. Each of the phosphoinositides of interest (All from Sigma) was added to the mixed solution at 1% w/w of the total lipid. The lipid solution was dried in a vacuum evaporator and re-hydrated in PBS to generate 25 mg/ml lipid suspension, which was subjected to sonication in an ice-cold bath for 15min. After the suspension became optically clear, it was diluted to 1 mg/ml lipid concentration.

In 1ml PBS, 2.5 μg of the purified GRAM domain was mixed with 0.25 mg-equivalent lipid suspension and incubated for 10min at room temperature. Then the mixture was centrifuged at 14,000rpm for 15min. The fluorescent intensity of the supernatant fraction was determined by RF-5300 PC spectrofluorophotometer (Shimazu).

Results

Partial purification of tagged GRAM protein.

For the following binding experiments, the GRAM domain of Paz4 was expressed as a fusion protein with GST and YFP. The expression is more efficient when the cells were IPTG-induced at 25°C than at 37 °C possibly because the YFP or GRAM part of the protein could be folded with higher efficiency at a lower temperature. The fusion protein was then partially purified using glutathione-conjugated resin.

Fig.8 shows the Coomasie Blue staining pattern of the purified fraction (lane 2). A 61 kDa band was clearly visible which was the estimated molecular size of the fusion protein, and in addition, there is a

minor band just beneath the band. It is possible that this minor band is a partially degraded or modified form of the original one. Following experiments were done using this partially-purified protein.

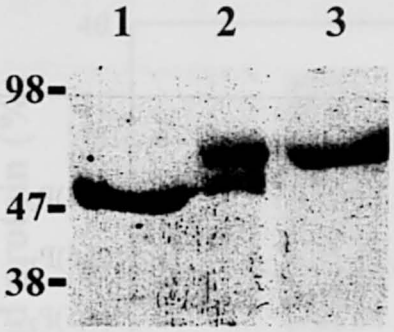

Fig.8 Electrophoresis pattern of partially-purified GST-YFP-GRAM protein.
Lane 1: GST-YFP purified in the same way as described for the GRAM-fusion protein.
Lane 2: GST-TFP-GRAM protein. Lane 3: GST-CFP (Cyan Fluorescent Protein)-FYVE protein.

Dot-blot assay for the tagged GRAM protein.

To asses the binding ability of GRAM domain to various species of lipids, the author employed the dot-blot assay. The partially-purified fraction of GRAM fusion protein was incubated with the nitrocellulose membrane (PIP Strips™) where 14 phospholipids and 1 sphingolipid had been spotted. The signal of the bound protein was visualized in the similar manner of immunoblot analysis.

Though the results of the repeated experiments are not exactly the same, they exhibited preferential binding signal toward some species of phosphoinositides. Fig.9 shows the representative pattern of the dot-blot analysis. The spots for PI (phosphatidylinositol), PI(4)P (phosphatidyl inositol 4'-monophosphate), and PI(5)P (phosphatidylinositol 5'-monophosphate) $_2$ became dense-colored compared to other spots. In contrast, the spots for PI(3)P (phosphatidyl inositol 3'-monophosphate) or PI(4,5)P_2 (phosphatidyl inositol 4', 5'-diphosphate) never gave positive

signal. This result is quite notable because other known membrane-binding domains are reported to have affinities toward either of the two species of phosphoinositide, PI(3)P or $PI(4,5)P_2$ (6, 12, 49).

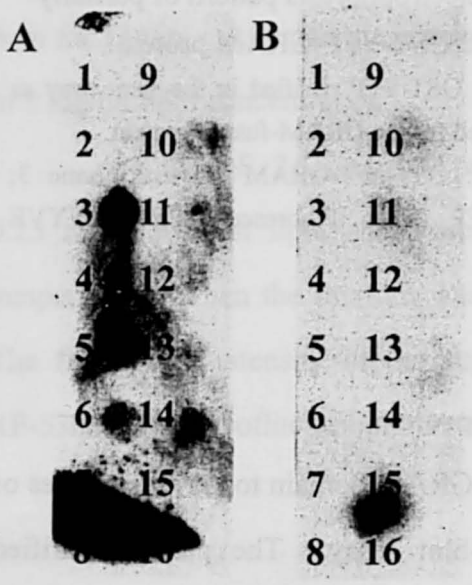

Fig.8 Dot-blot assay for the GST-YFP-GRAM protein.
(A) The signal pattern for the GST-YFP-GRAM protein. Strong signal was visible for PI, which were not detected in other trials. The spots for PI(4)P and PI(5)P had positive signals. (B) The signal pattern for the GST-YFP protein (without GRAM domain). There were no visible signals on the film. (C) The spotted lipids were shown. LPA, lysophosphatidic acid; LPC, lysophosphatidiylcholine; PE, phosphatidylethanolamine; PC, phosphatidylcholine; PA, phosphatidic acid. The numbers in the blankets following PI mean the positions of phospholyrated inositol hydroxyl residues.

PI(4)P binding was confirmed by liposome binding assay.

The binding reaction of a membrane-association domain can be well reconstituted when the counterpart (some specific lipid) is embedded in a lamella of a liposome (35). And one can examine the binding both

quantitatively and qualitatively using liposome as a carrier of the lipid of interest. Taking advantage of high sensitivity of fluorometric detection, the author devised an assay to characterize the binding of GRAM domain.

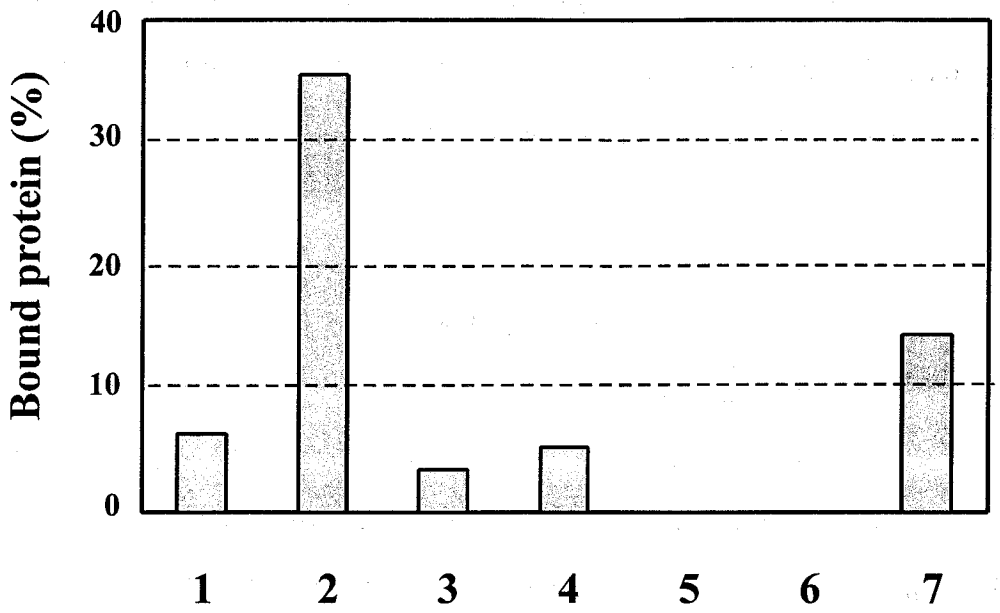

Fig.9 The binding profile for phosphoinositide-containing liposome of the GST-YFP-GRAM protein.

The GRAM fusion protein was mixed with liposomes containing 1% w/w of 1: PI(3)P; 2: PI(4)P; 3:PI(5)P; 4:PI(3,4)P_2; 5: PI(3,5)P_2; 6: PI(4,5)P_2; and 7: PI(3,4,5)P_3. The fluorescent intensity after the removal of the liposomes was determined and the decrease in the fluorescent intensity was expressed as percentage of that for the control fluorescent intensity (intensity determined after the mixture of the protein and liposome without any phosphoinositides). Only PI(4)P addition to the liposome substantially diminished the supernatant fluorescent intensity and gave significant value for the binding.

The partially-purified GST-YFP-GRAM protein was incubated with various phosphoinositides mixed in liposomes. Subsequently, membrane-bound GRAM protein was removed by centrifugation along with the liposome, and the fluorescent intensity of the supernatant part was

determined. Fig.9 shows the result of the assay. More than 35% of the mixed protein were able to be pulled down when the liposome contained 1%PI(4)P. The liposomes with the same amount of other phosphoinositides did not show obvious binding activities except for those with $PI(3,4,5)P_3$ which exhibited the removal of 15% of the protein. This result confirmed the dot-blot assay finding that GRAM domain can bind to PI(4)P.

Discussion

In combination with the results obtained by dot-blot assay, this liposome experiment indicates that PI(4)P was the potent binding partner of the GRAM protein of Paz4. For other species of phosphoinositides, PI(5)P, $PI(3,4)P_2$, and $PI(3,4,5)P_3$ showed ambiguous results, but PI(3)P and $PI(4,5)P_2$ did not show any positive binding signal for the protein. As mentioned above, the preferential binding of the GRAM protein to PI(4)P, not to PI(3)P or $PI(4,5)P_2$, is a unique feature among known domains for membrane association. The clear discrepancy of the binding properties between GRAM and other domains implies that this domain can contribute to some unique physiological functions. In *S.cerevisiae*, PI(4)P is synthesized from PI by the catalysis of either Stt4 or Pik1 lipid kinase, and the abnormal accumulation of PI(4)P caused by PI(4)P phosphatase SacI mutation leads to defects in Golgi function, lipid storage regulation, cytoskeleton organization, and most notably, in vacuolar morphology maintenance (11). So far the GRAM protein which the author found is an only one candidate for the specific binding partner for PI(4)P. Since

GRAM domain proteins are identified widely in eukaryotes, it is plausible that this domain has been evolutionally preserved as an important linker domain to recruit the host protein to the specific lipid.

Summary

The author identified Paz4/Ugt51 sterol glucosyltransferase as an essential factor in both micro- and macro-pexophagy in *P.pastoris*. The intactness of other autophagy processes in *paz4*-null mutants indicated that Paz4 is a unique Paz member in that it acts specifically on pexophagy processes. From AOD-degradation assays for strains with domain-deleted Paz4 variants, GRAM domain and Catalytic domain were discovered to be essential for the micropexophagy function of Paz4.

The localization study of the Paz4-variant expressing cells elucidated the role of GRAM domain as a localization determinant of the host protein. Point mutation of GRAM domain (Y642P) resulted in the same defects as the deletion of the whole domain did, indicating the importance of the tyrosine residue in the function of GRAM domain.

Finally, the biochemical study of the GRAM domain was carried out. Two different assay systems led to the conclusion that the GRAM domain has binding activity toward PI(4)P, but not toward PI(3)P or $PI(4,5)P_2$, showing clear distinguished properties of GRAM domain from those of other known domains for membrane association.

CHAPTER III

Visualization and role of actin cytoskeleton in pexophagy

Introduction

Cytoskeletons have diverse and essential functions such as maintenance of cell morphology, cell duplication, secretion, and cell movement, etc(4, 29, 32, 46). In yeasts, actin cytoskeleton plays dominant roles in their physiological functions. Recent studies have identified many factors associated in actin structures, which contribute to the regulation of organella transport systems. For instance, peroxisome inheritance to a budding daughter cell is dependent on actin-myosin molecular complex(15), and homotypic vacuolar fusion event was also reported to dependent on actin-related proteins(38). Pexophagic processes, especially micropexophagic processes, contain these organella movements and thus it is plausible that actin cytoskeleton is also involved in these processes.

The author employed two methods to investigate the role of actin cytoskeleton in micropexophagy. One was visualization of actin itself through the expression of GFP-tagged actin protein. The other method was so called an inhibitor experiment, in which a drug that disrupts actin polymerisation were added during micropexophagy induction. The results from these experiments highlighted a new actin-containing structure at the onset of micropexophagy and brought the evidence for actin involvement in micropexophagy.

Materials and methods

Observation of GFP-Act1 localization

P.pastoris ACT1 ORF gene (actin, GenBank™ accession number: AF216956) was PCR-amplified from *P. pastoris* wild type strain genome with 5'-ACT1 ORFPstI (AACTGCAGCCATCCACTTCCGGAGAGACG GAGGTAAGTCAGCTCTT) and 3'-ACT1ORFXhoI (CCGCTCGAGTTA GAAACACTTGAGGTGCACAA) as primers. The 5'- noncoding region of the *ACT1* gene was also PCR-amplified with primers called 5'-ACT1PRSacII (TCCCCGCGGTCGCTGGTAATCCCGGCTTTT) and 3'-ACT1PRPstI (AACTGCAGCATTGTATTGATGAATTTCTTTTACT). Both of the amplified DNA fragments were cloned into pHM100 (pBluescript SK+ containing *P. pastoris HIS4*) after restriction enzyme treatments (*Pst* I/ *Xho* I for ORF fragment and *Sac* II/ *Pst* I for 5'-noncoding region fragment), which gave pTN101. The *GFP* fragment was cut out by *Pst* I from pHM108 (See Table 2 in Chapter II), and ligated into pTN101. The resultant plasmid (pTN102), in which *GFP-ACT1* gene was located next to the 5'- noncoding region of *ACT1*, was linearized with *Stu* I and introduced to *P. pastoris* wild type strain PPY12, which generated strain TNP1.

The observation of GFP-Act1 along with the vacuolar membrane marker FM 4-64 was done in the same way as described in Chapter II.

Latrunculin A application

Latrunculin A which was reported to be a potent inhibitor of actin polymerisation (36) was purchased from Wako Chemical.

Methanol-grown cells (strain TNP1 or STW1) were treated with this drug at 100μM concentration upon the carbon source shift to glucose (SD medium). After incubation for the period indicated hereafter, the cells were subjected to fluorescent microscopy as described in Chapter II.

Results

Observation of GFP-Act1 localization change during micropexophagy.

P. pastoris Act1 tagged with GFP was expressed under its original promoter regulation. The cells were grown in SM medium to induce peroxisomes, and subsequently transferred to SD medium. The GFP image during the incubation was acquired along with vacuolar membrane marker (FM 4-64) signal.

Fig.1 shows the localization pattern of the GFP-tagged Act1 (middle panels). Interestingly, before the onset of micropexophagy (during incubation in SM medium), a few dot structures were seen inside the cell body (Fig.1A). The intracellular dots were often close to vacuolar membrane (left panels), and they were sensitive to Latrunculin A treatment (Fig.1B). In a previous study which observed GFP-Act1 pattern in *S. cerevisiae* during cell cycle (9), dot structures were detected only on the cell cortex (just beneath the cell surface) during vegetative growth. Thus it is suggested that the observed intracellular dots may be a peculiar structure to *P. pastoris* or methylotrophic yeasts only visible when the cells were grown on methanol.

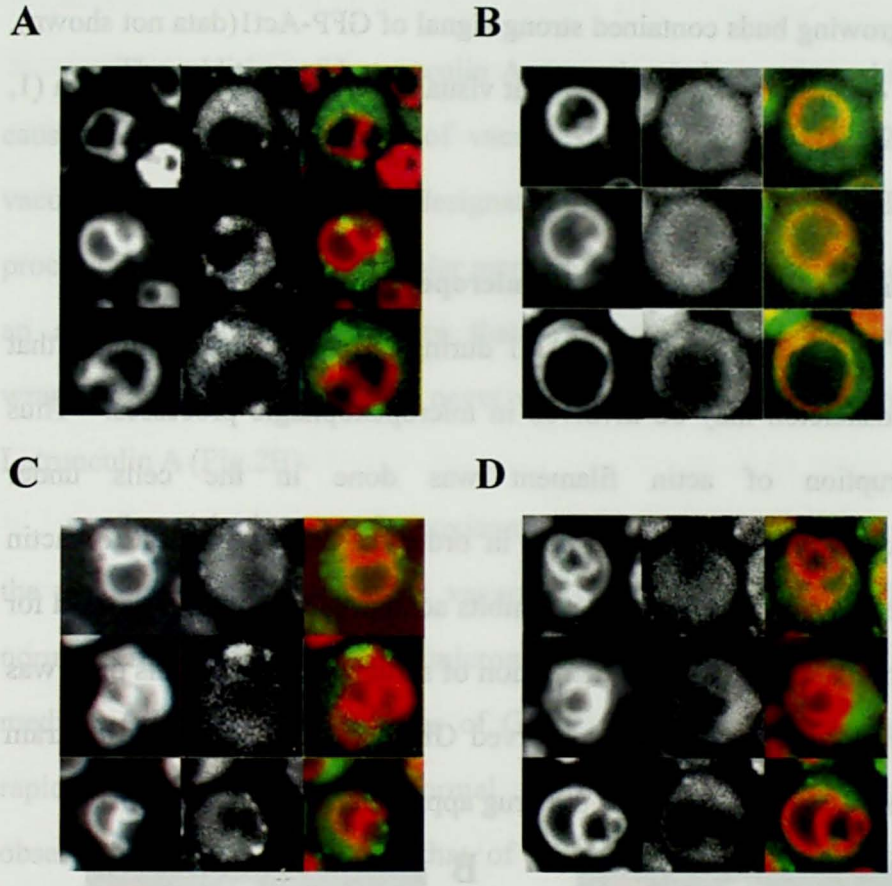

Fig.1 Localization of GFP-Act1 during micropexophagy.

Left panels, vacuolar membrane; middle panels, GFP-Act1 signal; and right panels, merged images. (A,B) Observation of strain TNP1 cells grown in SM medium. The dot structures of GFP-Act1 were seen inside the cells (A) which were eliminated by addition of 100 μM Latrunculin A (B). (C) The cells were transferred to SD medium for 5min. The number of the dot structures decreased rapidly. (D) After 3h incubation in SD medium, the intracellular dot structures completely disappeared.

The carbon source shift to glucose induced normal micropexophagic processes as judged by the change of vacuolar morphology. In the meantime, the dots of GFP-Act1 signal inside the cell body disappears rapidly (Fig.1C) and there were no visible dot structures in the cell body with deeply-invaginated vacuole (Fig.1D). The incipient bud

sites or growing buds contained strong signal of GFP-Act1(data not shown), which is consistent with the study that visualized the cortical actin patch (1, 9).

Actin-filament disruption inhibits micropexophagy.

The dynamics of GFP-Act1 during micropexophagy implies that actin cytoskeleton may be involved in micropexophagic processes. Thus the disruption of actin filament was done in the cells under micropexophagy-inducing condition in order to address the role of actin cytoskeleton. Latrunculin A that inhibits actin polymerisation was used for the purpose, and the effective disruption of actin structures by this drug was confirmed by the fact that the observed GFP-Act1 dot structures in strain TNP1 disappeared rapidly after the drug application (data not shown).

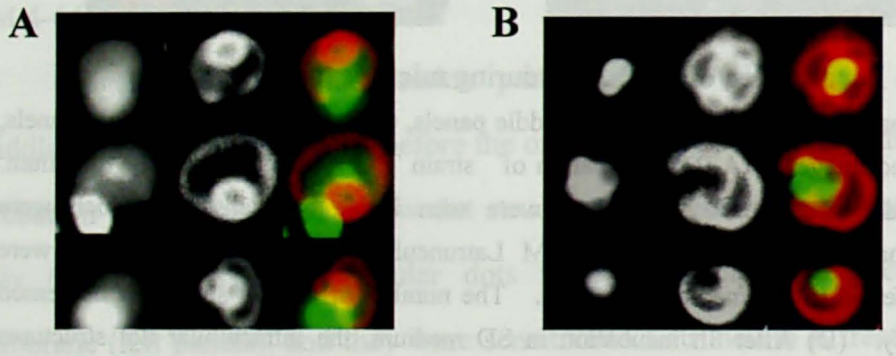

Fig.2 Micropexophagy was inhibited by actin-filament disruption.
Strain STW1 was grown on methanol and subsequently transferred to SD medium. The images were acquired 1h after the carbon source. Left panels, GFP-PTS1 signal; middle panels, vacuolar membrane signal (FM 4-64); and right panels, merged images. (A) In the existence of 100 μM Latrunculin A, the vacuolar engulfment of peroxisome cluster was not observed and a ring-shaped structure of vacuolar membrane was apparent uncoupled to peroxisome localization. (B) Without Latrunculin A, the cells exhibited normal micropexophagy progression.

The addition of Latrunculin A upon the carbon source shift to SD caused abnormal morphology of vacuole in strain STW1 (Fig.2A). The vacuolar engulfment processes designated as Stage 1 (See Chapter I) did not proceed normally, and the vacuolar membrane was often observed to contain an abnormal ring-like structure that was not engaged in peroxisome wrapping. This structure was never observed in the same strain without Latrunculin A (Fig.2B).

Surprisingly, part of peroxisome signal (GFP-PTS1) diffused inside the vacuolar lumen though the vacuolar membrane did not undergo the normal engulfment stage of micropexophagy in Latrunculin A-added medium (Fig.2A). The kinetics of GFP-signal diffusion was even more rapid than that under the normal micropexophagic condition. This observation image resembled that of macropexophagy progression (33). Thus the author assumed that the disruption of actin cytoskeleton inhibited micropexophagy and promoted macropexophagy instead.

Discussion

Through the GFP-Act1 expression in *P. pastoris*, the author observed the disappearance of dot structure from actin during micropexophagy (Fig.1). It is known that GFP-Act1 does not visualize all the actin cytoskeleton structure(9) and in our experiment actin cables were not observed. However, the GFP-Act1 dot pattern seems to reflect some endogeneous actin-cytoskeleton localization because it was eliminated by

Latrunculin A addition. Dot structures similar to those which the author found were observed in *S. cerevisiae* study when the cells were transferred to sporulation medium (9). The resemblance of the actin cytoskeleton structure between methanol-grown cells and sporulating cells is interesting in that the cells on both conditions undergo *de novo* organelle induction namely peroxisome or prospore membrane (47).

The disruption of actin cytoskeleton abolished vacuolar engulfment dynamics and gave rise to an abnormal vacuolar membrane structure (Fig.2A). The formation of this membrane structure was not coupled to peroxisome sequestration indicating that the drug treatment inhibited micropexophagy. On the other hand, macropexophagy seemed to be induced by the same treatment as judged by the diffused GFP signal pattern. This shows that intact actin cytoskeleton is specifically required for micropexophagy. Interestingly, the only one putative Paz factor specific to micropexophagy, Paz15, can interact with calmodulin, one of the constituents of actin-myosin complex (Aoyagi, personal communication). The combination of the studies of two factors, actin and Paz15, is needed to elucidate the actual role of actin cytoskeleton in micropexophagic processes.

Summary

Through the observation of GFP-Act1 dynamics, the author found the existence of dot-shaped actin structure in the cells grown on methanol, and the rapid disappearance of the structure during micropexophagy. The abnormal morphology of vacuolar membrane was observed when actin

polymerisation inhibitor Latrunculin A was applied to the cells shifted to glucose medium. The drug treatment abolished the vacuolar engulfment of peroxisome cluster and thus inhibited micropexophagy. The induction of macropexophagy-like peroxisome import into vacuolar lumen suggests the specific requirement of actin cytoskeleton for micropexophagy and the existence of other membrane dynamics compensating for the inhibition of micropexophagy.

CONCLUSION

The author studied peroxisome degradation system termed pexophagy in a methylotrophic yeast *Pichia pastoris*. One pathway of the pexophagic processes, micropexophagy, contains various membrane dynamics of vacuole and functions to maintain intracellular homeostasis in mammalian cells. Since micropexophagy is observed only in *P. pastoris* among yeasts, the author focused on the analysis of micropexophagy in this methylotrophic yeast taking advantage of its convenience in genetic manipulations.

The analyses were initiated by the morphological depiction of membrane dynamics in micropexophagy. Fluorescent staining methods of organelles in living cells in combination with cell-immobilizing technique enabled the author to trace the overall morphological change of vacuolar membrane during micropexophagy in a single cell. The observation led to finding of novel mode of vacuolar engulfment process along peroxisomes, namely vacuolar lobe formation. The schematic model of micropexophagy was modified based on the discovery, which gave the model that were able to explain all the observed images of wild-type or micropexophagy-defective cells. The micropexophagy-defective mutants designated as *paz* mutants were classified according to the modified model.

Next, the author analysed *PAZ4* encoding sterol glucosyltransferase Ugt51. Though the requirement of PAZ4 for pexophagy was confirmed in enzymatic and morphological experiments, the author found that the gene product is dispensable for nitrogen starvation-induced autophagic processes

unlike other Paz proteins. The GRAM domain as well as catalytic domain in Paz4 was shown to be essential for its micropexophagy function. Furthermore morphological analysis of GRAM domain-mutated Paz4 indicated that the domain act as the localization determinant of Paz4 during micropexophagy. After bacterial expression and purification the GRAM domain of Paz4 was subjected to biochemical analyses to investigate its binding properties. The author succeeded in the detection of binding ability of Paz4 GRAM domain to one of the biological important phosphoinositides, phosphatidylinositol 4'-monophosphate (PI(4)P). The biochemical feature of Paz4 GRAM domain gave an insight that the pexophagic processes can be regulated by phosphoinositide localization or turnover.

Finally the involvement of actin cytoskeleton in micropexophagy was investigated. In the course of GFP-Act1 (actin) localization study, the author found intracellular dot structures of actin that was specifically present before the micropexophagy induction. The disruption of actin filament caused abnormal vacuolar morphology (ring structure) irrelevant to peroxisome sequestration. The induction of macropexophagy-like mechanism after the disruption of actin filament suggested the specific involvement of intact actin cytoskeleton in micropexophagy.

REFERENCES

1. **Amberg, D.C.** 1998. Three-dimensional imaging of the yeast actin cytoskeleton through the budding cell cycle. Mol Biol Cell. **9:** 3259-3262.
2. **Baba, M., K. Takeshige, N. Baba, and Y. Ohsumi.** 1994. Ultrastructural analysis of the autophagic process in yeast: detection of autophagosomes and their characterization. J. Cell Biol. **124:** 903-913.
3. **Burd, C.G. and S.D. Emr.** 1998. Phosphatidylinositol(3)-phosphate signaling mediated by specific binding to RING FYVE domains. Molecular Cell. **2:** 157-162.
4. **Casanova, J.E.** 2002. Epithelial cell cytoskeleton and intracellular trafficking V. Confluence of membrane trafficking and motility in epithelial cell models. Am J Physiol Gastrointest Liver Physiol. **283:** G1015-G1019.
5. **Catlett, N.L. and L.S. Weisman.** 2000. Divide and multiply: organelle partitioning in yeast. Curr Opin Cell Biol. **12:** 509-516.
6. **De Camilli, P., H. Chen, J. Hyman, E. Panepucci, A. Bateman, and A.T. Brunger.** 2002. The ENTH domain. FEBS Lett. **513:** 11-18.
7. **de Gouyon, B.M., W. Zhao, J. Laporte, J.L. Mandel, A. Metzenberg, and G.E. Herman.** 1997. Characterization of mutations in the myotubularin gene in twenty six patients with X-linked myotubular myopathy. Hum Mol Genet. **6:** 1499-1504.
8. **Doerks, T., M. Strauss, M. Brendel, and P. Bork.** 2000. GRAM, a novel domain in glucosyltransferases, myotubularins and other putative membrane-associated proteins. Trends Biochem Sci. **25:** 483-485.
9. **Doyle, T. and D. Botstein.** 1996. Movement of yeast cortical actin cytoskeleton visualized in vivo. Proc Natl Acad Sci U S A. **93:** 3886-3891.
10. **Fosse, M., T.O. Berg, D.S. O'Reilly, and P.O. Seglen.** 1995. Vanadate inhibition of hepatocytic autophagy. Calcium-modulated and osmolality-modulated antagonism by asparagine. Eur J Biochem. **230:**

17-24.

11. **Foti, M., A. Audhya, and S.D. Emr.** 2001. Sac1 lipid phosphatase and Stt4 phosphatidylinositol 4-kinase regulate a pool of phosphatidylinositol 4-phosphate that functions in the control of the actin cytoskeleton and vacuole morphology. Mol Biol Cell. **12:** 2396-2411.
12. **Gaullier, J.M., A. Simonsen, A. D'Arrigo, B. Bremnes, H. Stenmark, and R. Aasland.** 1998. FYVE fingers bind PtdIns(3)P. Nature. **394:** 432-433.
13. **Gordon, P.B., I. Holen, M. Fosse, J.S. Rotnes, and P.O. Seglen.** 1993. Dependence of hepatocytic autophagy on intracellularly sequestered calcium. J Biol Chem. **268:** 26107-26112.
14. **Harding, T.M., G.A. Hefner, M. Thumm, and D.J. Klionsky.** 1996. Genetic and phenotypic overlap between autophagy and the cytoplasm to vacuole protein targeting pathway. J Biol Chem. **271:** 17621-17624.
15. **Hoepfner, D., M. van den Berg, P. Philippsen, H.F. Tabak, and E.H. Hettema.** 2001. A role for Vps1p, actin, and the Myo2p motor in peroxisome abundance and inheritance in Saccharomyces cerevisiae. Journal of Cell Biology. **155:** 979-990.
16. **Hutchins, M.U., M. Veenhuis, and D.J. Klionsky.** 1999. Peroxisome degradation in *Saccharomyces cerevisiae* is dependent on machinary of macroautophagy and the Cvt pathway. J. Cell Sci. **112:** 4079-4087.
17. **Kadowaki, M., R. Venerando, G. Miotto, and G.E. Mortimore.** 1996. Mechanism of autophagy in permeabilized hepatocytes: evidence for regulation by GTP binding proteins. Adv Exp Med Biol. **389:** 113-119.
18. **Kato, M. and W. Wickner.** 2001. Ergosterol is required for the Sec18/ATP-dependent priming step of homotypic fusion. EMBO Journal. **20:** 4035-4040.
19. **Kim, J., V.M. Dalton, K.P. Eggerton, S.V. Scott, and D.J. Klionsky.** 1999. Apg7p/Cvt2p is required for the cytoplasm-to vacuole targeting, macroautophagy, and peroxisome degradation pathways. Mol. Biol. Cell. **10:** 1337-1351.

20. **Kim, S.A., G.S. Taylor, K.M. Torgersen, and J.E. Dixon.** 2002. Myotubularin and MTMR2, phosphatidylinositol 3-phosphatases mutated in myotubular myopathy and type 4B Charcot-Marie-Tooth disease. J Biol Chem. **277:** 4526-4531.
21. **Kim, Y.K., Y. Wang, Z.M. Liu, and P.E. Kolattukudy.** 2002. Identification of a hard surface contact-induced gene in Colletotrichum gloeosporioides conidia as a sterol glycosyl transferase, a novel fungal virulence factor. Plant J. **30:** 177-187.
22. **Laporte, J., F. Blondeau, A. Buj-Bello, and J.L. Mandel.** 2001. The myotubularin family: from genetic disease to phosphoinositide metabolism. Trends Genet. **17:** 221-228.
23. **Lemmon, M.A. and K.M. Ferguson.** 2000. Pleckstrin homology domains: phosphoinositide-regulated membrane tethers, in Biology of Phosphoinositides, edit. S. Cockcroft, Oxford University Press, London: 131-165.
24. **Mortimore, G.E., N.J. Hutson, and C.A. Surmacz.** 1983. Quantitative correlation between macro- and microautophagy in mouse hepatocytes during starvation and refeeding. Proc. Natl. Acad. Sci. USA. **80:** 2179-2183.
25. **Mortimore, G.E., B.R. Lardeux, and C.E. Adams.** 1988. Regulation of microautophagy and basal protein turnover in rat liver: Effects of short-term starvation. J. Biol. Chem. **263:** 2506-2512.
26. **Mukaiyama, H., M. Oku, T. Samizo, A.T. Hammond, B.S. Glick, N. Kato, and Y. Sakai.** 2002. Paz2 and 13 other PAZ gene products regulate vacuolar engulfment of peroxisomes during micropexophagy. Genes Cells. **7:** 75-90.
27. **Noda, T., J. Kim, W.-P. Huang, M. Baba, C. Tokunaga, Y. Ohsumi, and D.J. Klionsky.** 2000. Apg9p/Cvt7p is an integral membrane protein required for transport vesicle formation in the Cvt and autophagy pathways. J. Cell Biol. **148:** 465-479.
28. **Noda, T., A. Matsuura, Y. Wada, and Y. Ohsumi.** 1995. Novel system for monitoring autophagy in the yeast *Saccharomyces cerevisiae.* Biochem. Biophys. Res. Commun. **210:** 126-32.

29. **Noguchi, T., R. Arai, F. Motegi, K. Nakano, and I. Mabuchi.** 2001. Contractile ring formation in Xenopus egg and fission yeast. Cell Struct Funct. **26:** 545-554.

30. **Peng, L., Y. Kawagoe, P. Hogan, and D. Delmer.** 2002. Sitosterol-b-glucoside as primer for cellulose synthesis in plants. Science. **295:** 147-150.

31. **Peters, J.M.** 2002. The anaphase-promoting complex: proteolysis in mitosis and beyond. Mol Cell. **9:** 931-943.

32. **Pruyne, D. and A. Bretscher.** 2000. Polarization of cell growth in yeast. J Cell Sci. **113:** 571-585.

33. **Sakai, Y., A. Koller, L.K. Rangell, G.A. Keller, and S. Subramani.** 1998. Peroxisome degradation by microautophagy in *Pichia pastoris*: identification of specific steps and morphological intermediates. J. Cell Biol. **141:** 625-636.

34. **Sakai, Y. and S. Subramani.** 2000. Environmental response of yeast peroxisomes: aspects of organelle assembly and degradation. Cell Biochem. Biophys. **32:** 51-61.

35. **Sankaran, V.G., D.E. Klein, M.M. Sachdeva, and M.A. Lemmon.** 2001. High-affinity binding of a FYVE domain to phosphatidylinositol 3-phosphate requires intact phospholipid but not FYVE domain oligomerization. Biochemistry. **40:** 8581-8587.

36. **Schatten, G., H. Schatten, I. Spector, C. Cline, N. Paweletz, C. Simerly, and C. Petzelt.** 1986. Latrunculin inhibits the microfilament-mediated processes during fertilization, cleavage and early development in sea urchins and mice. Exp Cell Res. **166: 191-208.**

37. **Scott, S.V., G.A. Hefner, K.A. Morano, T. Noda, Y. Ohsumi, and D.J. Klionsky.** 1996. Cytoplasm-to-vacuole targeting and autophagy employ the same machinery to deliver proteins to the yeast vacuole. Proc Natl Acad Sci U S A. **93:** 12304-12308.

38. **Seeley, E.S., M. Kato, N. Margolis, W. Wickner, and G. Eitzen.** 2002. Genomic analysis of homotypic vacuole fusion. Mol Biol Cell. **13:** 782-794.

39. **Takeshige, K., M. Baba, S. Tsuboi, T. Noda, and Y. Ohsumi.** 1992. Autophagy in yeast demonstrated with proteinase-deficient mutants and conditions for its induction. J. Cell Biol. **119:** 301-311.
40. **Tanaka, K.** 2001. [Ubiquitin and proteasome]. Tanpakushitsu Kakusan Koso. **46:** 1697-1703.
41. **Titorenko, V., I., I. Keizer, W. Harder, and M. Veenhuis.** 1995. Isolation and characterization of mutants impaired in the selective degradation of peroxisomes n the yeast *Hansenula polymorpha.* J. Bacteriol. **177:** 357-363.
42. **Tsukada, M. and Y. Ohsumi.** 1993. Isolation and characterization of autophagy-defective mutants of Saccharomyces cerevisiae. FEBS Lett. **333:** 169-174.
43. **Tuttle, D.L. and W.A. Dunn.** 1995. Divergent modes of autophagy in the methylotrophic yeast *Pichia pastoris.* J. Cell Sci. **108:** 25-35.
44. **Tuttle, D.L., A.S. Lewin, and W.A.J. Dunn.** 1993. Selective autophagy of peroxisomes in methylotrophic yeasts. Eur. J. Cell Biol. **60:** 283-290.
45. **Warnecke, D., R. Erdmann, A. Fahl, B. Hube, F. Muller, T. Zank, U. Zahringer, and E. Heinz. 1999.** Cloning and functional expression of UGT genes encoding sterol glucosyltransferases from *Saccharomyces cerevisiae, Candida albicans, Pichia pastoris*, and *Dictyostelium discoideum.* J. Biol. Chem. **274:** 13048-13059.
46. **Westphal, M., A. Jungbluth, M. Heidecker, B. Muhlbauer, C. Heizer, J.M. Schwartz, G. Marriott, and G. Gerisch.** 1997. Microfilament dynamics during cell movement and chemotaxis monitored using a GFP-actin fusion protein. Curr Biol. **7:** 176-183.
47. **Whitacre, J., D. Davis, K. Toenjes, S. Brower, and A. Adams.** 2001. Generation of an isogenic collection of yeast actin mutants and identification of three interrelated phenotypes. Genetics. **157:** 533-543.
48. **Wishart, M.J. and J.E. Dixon.** 2002. PTEN and myotubularin phosphatases: from 3-phosphoinositide dephosphorylation to disease. Phosphatase and tensin homolog deleted on chromosome ten. Trends Cell Biol. **12:** 579-585.

49. **Xu, Y., L.F. Seet, B. Hanson, and W. Hong.** 2001. The Phox homology (PX) domain, a new player in phosphoinositide signalling. Biochem J. **360:** 513-530.

50. **Yuan, W., P.E. Stromhaug, and W.A.J. Dunn.** 1999. Glucose-induced autophagy of peroxisomes in *Pichia pastoris* requires a unique E1-like protein. Mol. Biol. Cell. **10:** 1353-1366.

ACKNOWLEDGEMENTS

The author wishes to express many sincere thanks to Professor Nobuo Kato, Kyoto University, for his kind guidance, valuable discussions, and continuous warm encouragement during the course of this study.

The author would like to express many hearty thanks to Associate Professor Yasuyoshi Sakai, Kyoto University, for his directions of this study, valuable discussions, and warm encouragement during the course of this study.

The author acknowledges Professor Yoshinori Ohsumi and Dr. Takeshi Noda, National Institute for Basic Biology, for their significant discussions and for supplementing some strains of *Saccharomyces cerevisiae*.

The author dedicates special thanks to Dr. Dirk Warnecke, University of Hamburg, for enormous discussions, for providing some DNA samples, and for the thin layer chromatography analysis in the study on Paz4.

The author would like to express great gratitude to Associate Professor Kazumitsu Ueda, Kyoto University, for technical advice in the preparation of liposomes.

The author is grateful to all members of Laboratory of Microbial Biotechnology, Division of Applied Life Sciences, Graduate School of Agriculture, Kyoto University, for their friendliness and cooperativeness through this study.

In the end of these acknowledgements, the author would like to express sincere feelings of appreciation toward his family, especially to his

wife Haruna Oku, for their continuous encouragements and patient supports during this study.